PHYSICAL REVIEW D **88,** 015025 (2013)

Dark matter detection in focus point supersymmetry

Patrick Draper,[1,2,*] Jonathan L. Feng,[3] Philipp Kant,[4,†] Stefano Profumo,[1,2,‡] and David Sanford[5,§]

[1]*Department of Physics, University of California, 1156 High Street, Santa Cruz, California 95064, USA*
[2]*Santa Cruz Institute for Particle Physics, Santa Cruz, California 95064, USA*
[3]*Department of Physics and Astronomy, University of California, Irvine, California 92697, USA*
[4]*Humboldt-Universität zu Berlin, 12489 Berlin, Germany*
[5]*California Institute of Technology, Pasadena, California 91125, USA*

(Received 11 April 2013; published 23 July 2013)

We determine the prospects for direct and indirect detection of thermal relic neutralinos in supersymmetric theories with multi-TeV squarks and sleptons. We consider the concrete example of the focus point region of minimal supergravity, but our results are generically valid for all models with decoupled scalars and mixed Bino-Higgsino or Higgsino-like dark matter. We determine the parameter space consistent with a 125 GeV Higgs boson including 3-loop corrections in the calculation of the Higgs mass. These corrections increase m_h by 1–3 GeV, lowering the preferred scalar mass scale and decreasing the fine-tuning measure in these scenarios. We then systematically examine prospects for dark matter direct and indirect detection. Direct detection constraints do not exclude these models, especially for $\mu < 0$. At the same time, the scenario generically predicts spin-independent signals just beyond current bounds. We also consider indirect detection with neutrinos, gamma rays, antiprotons, and antideuterons. Current IceCube neutrino constraints are competitive with direct detection, implying bright prospects for complementary searches with both direct and indirect detection.

DOI: 10.1103/PhysRevD.88.015025 PACS numbers: 12.60.Jv, 14.80.Da, 95.35.+d

I. INTRODUCTION

There are now many experimental constraints on weak-scale supersymmetry. These exclude generic supersymmetric theories in which all superpartners have masses below a TeV, and focus attention on the remaining supersymmetric theories that are both phenomenologically viable and natural. In this work, we consider focus point supersymmetry [1,2], in which multi-TeV squarks and sleptons are hierarchically heavier than the other superpartners.

Focus point models are motivated by a variety of considerations. Heavy first and second generation sfermions help satisfy low-energy constraints on flavor and CP violation, and heavy third generation sfermions raise the Higgs boson mass to the required level of 125 GeV [3,4]. There are also theoretical reasons for expecting scalar superpartners to be heavier than the gauginos. For example, such a hierarchy results from an approximate $\mathrm{U}(1)_R$ symmetry [2] or if none of the supersymmetry-breaking fields is a complete gauge singlet [5,6]. Note also that gaugino masses enter the scalar mass renormalization group (RG) equations, but scalar masses do not enter the gaugino mass RG equations; letting $M_{1/2}$ and m_0 denote generic gaugino and scalar masses, respectively, the hierarchy $m_0 \gg M_{1/2}$ is therefore stable under RG evolution, whereas $M_{1/2} \gg m_0$ is not. Last, although large supersymmetry-breaking parameters are generically associated with significant fine-tuning of the Higgs potential, simple correlations in high-scale scalar mass parameters may reduce the sensitivity of the weak scale to variations in these parameters, providing a naturalness motivation for such models.

In this work, we consider in detail prospects for dark matter detection in such theories [7,8]. For concreteness, we consider the focus point region of minimal supergravity (mSUGRA), but the results are far more general: when the scalar superpartners are very heavy, they effectively decouple from dark matter phenomenology, and the details of the multi-TeV spectrum are largely irrelevant. The phenomenology of focus point dark matter encompasses the phenomenology of mixed Bino-Higgsino and pure Higgsino neutralino dark matter, and our conclusions for dark matter detection are generically valid for any model with heavy scalars where the Bino soft-supersymmetry breaking mass is lower than the Wino mass.

In Sec. II, we explain our treatment of mSUGRA parameter space. We then turn to the Higgs mass in Sec. III. There have been many studies of mSUGRA after the Higgs discovery; see, e.g. Refs. [9–12]. In contrast to these, here we include a 3-loop calculation of the Higgs mass using the public code H3M [13,14]. We find that 3-loop contributions raise the Higgs mass by 1–3 GeV over 2-loop results. Given the logarithmic sensitivity of the Higgs mass to the top squark mass, this lowers the preferred range of stop masses considerably. In this calculation stop masses as low as 3 TeV are consistent with the measured Higgs mass, even without significant stop left-right mixing. In the focus point parameter space, this correlates with a gluino as light as 2 TeV.

*pidraper@ucsc.edu
†philipp.kant@physik.hu-berlin.de
‡profumo@ucsc.edu
§dsanford@caltech.edu

We then consider prospects for dark matter detection in the region of parameter space preferred by the Higgs mass and other phenomenological constraints, including direct searches for supersymmetric particles. In Sec. IV, we discuss both spin-independent and spin-dependent direct detection and show that, contrary to claims in the literature, perfectly viable regions of parameter space remain, especially for $\mu < 0$. Crucial to this conclusion is the small value for the strange quark content of the nucleon now preferred by both lattice calculations and chiral perturbation theory results. At the same time, the scenario generically predicts spin-independent cross sections $\sigma_p^{\rm SI} \sim 1\,{\rm zb} = 10^{-9}\,{\rm pb} = 10^{-45}\,{\rm cm}^2$, implying that dark matter candidates in this class of theories might very well be discovered by direct detection experiments in the near future.

In Secs. V, VI, and VII, we analyze the implications for indirect detection with neutrinos, gamma rays, and antimatter, respectively. Although gamma rays and antimatter are currently not very constraining in focus point scenarios, current bounds from observations of neutrinos from the direction of the Sun with IceCube are stringent, and future runs with planned upgrades will probe much of the preferred region, providing an exciting, and in many respects orthogonal, complement to direct detection. In Sec. VIII, we discuss our results and conclude.

II. PARAMETER SPACE AND LHC SUPERPARTNER SEARCHES

The defining feature of focus point supersymmetry is the insensitivity of the weak scale to variations in the fundamental supersymmetry-breaking parameters, even in the presence of multi-TeV soft supersymmetry-breaking parameters. Focus point supersymmetry accommodates a range of thermal relic neutralinos that vary continuously from ~100 GeV Bino-Higgsino mixtures to heavier and more Higgsino-like neutralinos, culminating in Higgsino-like neutralinos with masses around 1 TeV [7,15]. Given the appeal of neutralino dark matter, it is natural to impose the thermal relic density as a constraint on the parameters space. In the context of mSUGRA, this constraint allows for a departure from the typical $(m_0, M_{1/2})$ parameter space—in which the cosmologically viable region is only a small sliver—to a parameter space in which every point is cosmologically viable and more parameters can be examined [16]. This parameter space is particularly relevant in light of the first three years of LHC results, which have effectively eliminated the so-called "bulk" scenario for neutralino dark matter with light scalars and severely constrained coannihilation scenarios with light scalars, while leaving the focus point relatively unscathed and strong as a possibility for neutralino dark matter.

In mSUGRA, the relic density constraint can be cast as the requirement that

$$\Omega_\chi(m_0, M_{1/2}, A_0, \tan\beta, {\rm sign}(\mu)) = \Omega_{\rm DM}, \qquad (1)$$

where $\Omega_{\rm DM} \simeq 0.23$ [17,18] is the dark matter density in units of the critical density. Focus point supersymmetry is possible with large A parameters [19], but given the motivations of simplicity, the hierarchy between supersymmetry-breaking parameters enforced by an approximate $U(1)_R$ symmetry, and the prediction of suppressed A terms in some high-energy frameworks [20,21], we choose $A_0 = 0$ throughout. We may then use Eq. (1) to solve for m_0 and present results in the $(\tan\beta, M_{1/2})$ plane for both signs of μ, with every point in these planes having the correct relic density. In general, Eq. (1) may be satisfied by more than one value of m_0; for example, there may be a coannihilation solution at low m_0 and a focus point solution at larger m_0. In such cases, we always use the largest allowed value of m_0.

Figure 1 shows contours of m_0 in the $(\tan\beta, M_{1/2})$ for points satisfying the relic density constraint, using SOFTSUSY 3.1.7 [22] to generate the SUSY spectrum and MICROMEGAS 2.4 [23] to calculate the relic density. These solutions for m_0 are found for low values of $|\mu|$ located near the $\mu^2 < 0$ region, where radiative electroweak symmetry breaking fails. The $\mu^2 < 0$ region moves to higher m_0 for increasing $M_{1/2}$ and decreasing $\tan\beta$ due to RG effects, and this behavior is reflected in the m_0 contours. In Fig. 1 the shaded region with low $M_{1/2}$ is excluded by ATLAS searches for jets + missing energy [24]. The other shaded regions, which will appear in all of our figures, include a region at large $\tan\beta$, where the RG evolution in SOFTSUSY becomes unreliable, and a region at large $M_{1/2}$ for $\mu < 0$, where numerical issues with loop corrections to neutralino masses make the solution algorithm for Ω unreliable. We stress that these last two regions are excluded not by theoretical or experimental constraints, but rather because numerical complications hinder our ability to make accurate predictions.

Since the sfermion sector is decoupled in focus point supersymmetry, the properties of neutralino dark matter are determined primarily by its mass and the amount of Bino-Higgsino mixing present. If the gauge eigenstate composition of the lightest neutralino is given by

$$\chi = a_{\tilde B}(-i\tilde B) + a_{\tilde W}(-i\tilde W) + a_{\tilde H_d}\tilde H_d + a_{\tilde H_u}\tilde H_u, \qquad (2)$$

with $a_{\tilde W} \ll 1$ in the focus point region, the dominant processes for both annihilation and scattering are proportional to either $(a_{\tilde B} a_{\tilde H_{u,d}})^2$ or $(a_{\tilde H_{u,d}})^4$ [16]. Since $|a_{\tilde H_u}| \sim |a_{\tilde H_d}|$, the mixing can be usefully parametrized by the Bino content $a_{\tilde B}$. Figure 2 contains contours of m_χ and $a_{\tilde B}$ consistent with $\Omega_\chi = \Omega_{\rm DM}$. For much of the parameter space, the neutralino dark matter is a Bino-Higgsino mixture, but as $M_{1/2}$ increases, m_χ increases, and $a_{\tilde B}$ decreases: the increasing Higgsino content compensates for the suppression of the annihilation cross section by larger neutralino masses to keep the thermal relic density constant. The behavior is similar for both signs of μ, though $a_{\tilde B}$ is somewhat larger

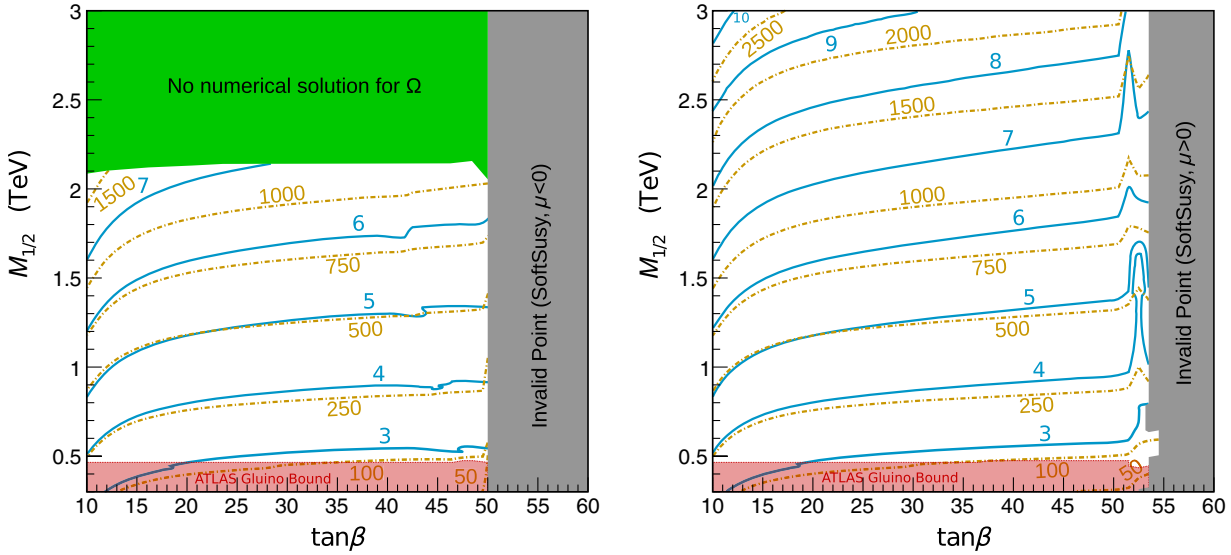

(a) $\mu < 0$ (b) $\mu > 0$

FIG. 1 (color online). Contours of m_0 in TeV (solid blue) and fine-tuning parameter c (dot-dashed gold) in the (tan β, $M_{1/2}$) plane for $\Omega_\chi \simeq 0.23$, $A_0 = 0$ and $\mu < 0$ (left) and $\mu > 0$ (right). The red shaded regions at low $M_{1/2}$ are excluded by the ATLAS gluino bound [24]. In the gray shaded regions at large tan β, the RG evolution in SOFTSUSY becomes unreliable, and in the green shaded region at large $M_{1/2}$ for $\mu < 0$, numerical issues with loop corrections to neutralino masses make the solution algorithm for Ω unreliable.

in the $\mu < 0$ case relative to the $\mu > 0$ due to the relative signs of $a_{\tilde{H}_{u,d}}$ for different signs of μ. In the limit of large $M_{1/2}$, the neutralino becomes nearly pure Higgsino with $a_{\tilde{B}} \to 0$, and the neutralino mass reaches $m_\chi \approx 1$ TeV.

In focus point scenarios, the weak scale is relatively insensitive to variations in supersymmetry breaking parameters, allowing for improved naturalness even with multi-TeV sfermion masses. There are many prescriptions for quantifying this naturalness, all of which are subject to significant subjective choices; for a review, see Ref. [25]. Here we use a naturalness measure based on the sensitivity coefficients [26,27]

$$c_a \equiv \left| \frac{\partial \ln m_Z^2}{\partial \ln a^2} \right|, \tag{3}$$

where a^2 is one of the input GUT-scale parameters m_0^2, $M_{1/2}^2$, A_0^2, μ_0^2, and m_3^2, the $H_u^0 H_d^0$ soft mass parameter. The overall fine-tuning of a model is defined as

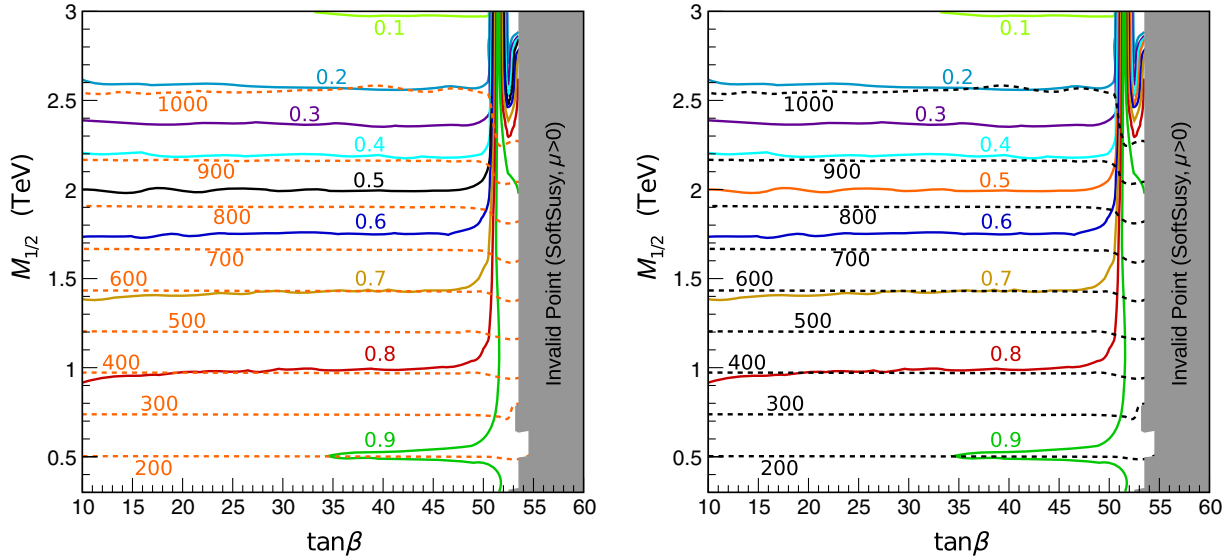

(a) $\mu < 0$ (b) $\mu > 0$

FIG. 2 (color online). Contours of m_χ in GeV (black dotted) and $|a_{\tilde{B}}|$ (solid colored).

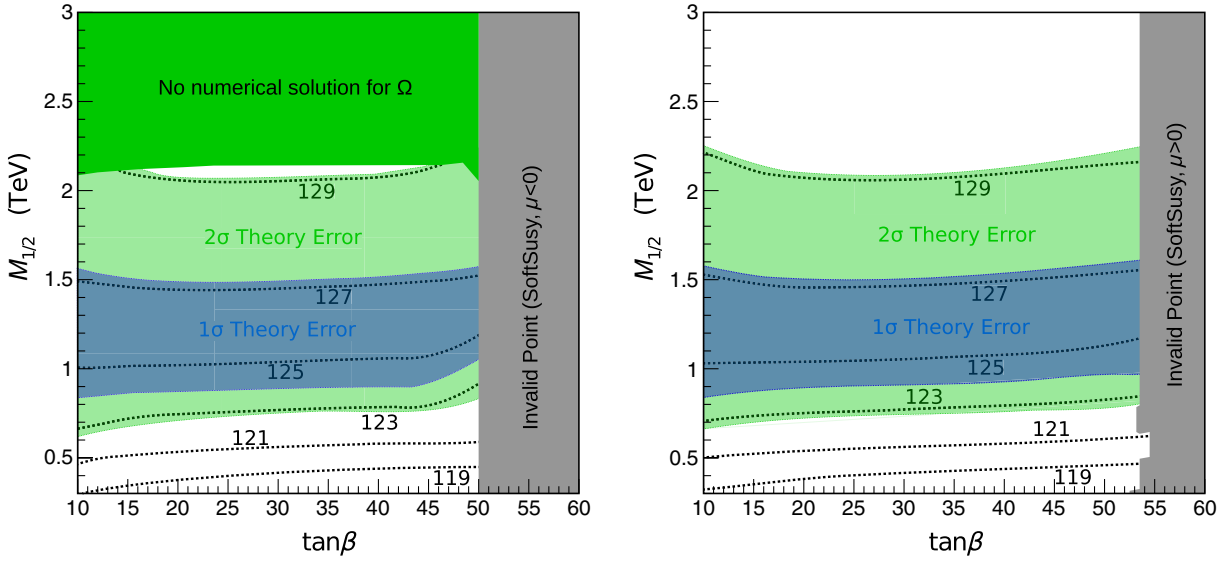

(a) $\mu < 0$ (b) $\mu > 0$

FIG. 3 (color online). Contours of m_h in GeV. In the shaded regions, the theoretical prediction for m_h is within 1σ and 2σ of the experimental central value $m_h = 125.5$ GeV, where $\sigma^2 \equiv \Delta_{\rm th}^2 + (1\ {\rm GeV})^2$.

$$c \equiv \max\{c_a\}, \tag{4}$$

and contours of c are shown in Fig. 1. In the explored region, c_{m_0} is always the largest sensitivity coefficient, and contours of c roughly follow contours of m_0, with values of $m_0 \sim 4$ TeV corresponding roughly to $c \sim 250$. A subset of the mSUGRA boundary conditions implies focusing, and the values of c shown in Fig. 1 are much smaller than would be expected without the focus point behavior.

III. CONSTRAINTS FROM THE HIGGS MASS

The mass of the recently discovered SM-like Higgs boson [3,4] provides a stringent constraint on the parameter space of any supersymmetric model. The most recent mass measurements are [28,29]

$$\text{ATLAS } 4\ell\text{: } 124.3^{+0.6+0.5}_{-0.5-0.3}\ \text{GeV}, \tag{5}$$

$$\text{ATLAS } \gamma\gamma\text{: } 126.8 \pm 0.2 \pm 0.7\ \text{GeV}, \tag{6}$$

$$\text{CMS } 4\ell\text{: } 125.8 \pm 0.5 \pm 0.2\ \text{GeV}, \tag{7}$$

$$\text{CMS } \gamma\gamma\text{: } 125.4 \pm 0.5 \pm 0.6\ \text{GeV}, \tag{8}$$

where the first uncertainties are statistical and the second uncertainties are systematic.

We calculate the lightest Higgs mass in the focus point region of mSUGRA with the program H3M, which calculates m_h in the $\overline{\rm DR}$ scheme including the dominant 3-loop contributions at $\mathcal{O}(\alpha_t\alpha_s^2)$ [13,14]. In addition, we modified H3M to increase the precision in the calculation of the running $\overline{\rm DR}$ top quark mass.[1] We set $m_t^{\rm pole} = 173.2$ GeV and $\alpha_s(m_Z) = 0.1184$, and fix the renormalization scale to the geometric mean of the stop masses. For further details, see Ref. [30].

In Fig. 3, we plot contours of m_h in the parameter space defined by Fig. 1. We find that the 3-loop terms generate a 1–3 GeV increase in m_h over the 2-loop truncation. The 2-loop terms in turn generate a 5–8 GeV increase over the 1-loop truncation, indicating convergence of the series. We observe also that the improved treatment of $m_t^{\overline{\rm DR}}$ and $\alpha_s^{\overline{\rm DR}}$ increases the 2-loop prediction relative to FEYNHIGGS [31–34]. For comparison, note that the geometric mean of the stop masses ranges from about 1 TeV at low $M_{1/2}$ to 8 TeV at high $M_{1/2}$ in the plotted parameter space.

In Fig. 3 we shade regions where the difference between the calculated m_h and the tentative central value 125.5 GeV is within the indicated theoretical uncertainty in the calculation. At each point on the parameter space, we assign a theoretical error bar $\Delta_{\rm th}$, defined as

$$\begin{aligned}\Delta_{\rm th} &\equiv \sqrt{(\Delta_{\rm pert})^2 + (\Delta_{\rm para})^2},\\ \Delta_{\rm pert} &\equiv \frac{1}{2}|m_h^{(3\text{-loop})} - m_h^{(2\text{-loop})}|,\\ \Delta_{\rm para} &\equiv m_h(m_t = 174.2\ \text{GeV}) - m_h(m_t = 173.2\ \text{GeV}).\end{aligned} \tag{9}$$

The uncertainty $\Delta_{\rm pert}$ from higher-order terms in the perturbation series is estimated to be in the range

[1]These changes are incorporated in the current version of H3M, which has been released simultaneously with Ref. [30].

0.5–1.5 GeV.[2] The parametric uncertainty $\Delta_{\rm para}$ induced by the uncertainty in the top quark mass is typically of order 0.5–1 GeV in the focus point parameter space.

The positive 3-loop terms significantly impact the preferred range of superpartner masses. Requiring that the theoretical prediction be within $\sqrt{\Delta_{\rm th}^2 + (1\ {\rm GeV})^2}$ of 125.5 GeV (where we have included a representative experimental uncertainty of 1 GeV based on the difference between ZZ and $\gamma\gamma$ channels at ATLAS), scalar mass parameters as low as $m_0 \sim 4$ TeV, corresponding to stop masses as low as 3 TeV, and gluino masses as low as $m_{\tilde{g}} \approx 2.8 M_{1/2} \sim 2$ TeV are consistent with the measured Higgs mass. Note that, combining the results shown in Figs. 1 and 3, the 3-loop m_h contributions also decrease allowed values of the fine-tuning parameter c by a factor of $\sim$5.

IV. DIRECT DARK MATTER DETECTION

It is well known that thermally produced neutralinos can possess a wide range of direct detection cross sections, from those that are significantly excluded to those that are orders of magnitude below current sensitivities. However, this full range of cross sections is not generic. Highly suppressed direct detection is typically associated with pure Bino scenarios, which have the correct thermal relic density only if there are light sfermions, coannihilation, or resonant annihilation through the pseudoscalar Higgs resonance. The first two possibilities are disfavored by the nonobservation of light squarks at the LHC, while the third depends upon careful tuning of the pseudoscalar Higgs mass to $m_A \approx 2m_\chi$. Most of the remaining parameter space is populated by models with Bino-Higgsino mixing like that found in the focus point region. For these models, the Bino-Higgsino mixing also sets the spin-independent neutralino-proton scattering cross section, which falls in the range $\sigma_p^{\rm SI} \sim 1$–40 zb for a wide range of model parameters when neutralinos have the right thermal relic density [16]. This range of cross sections is particularly relevant for current and near-future direct detection experiments; the XENON100 experiment [36,37] has begun probing this range of relevant cross sections, and near-future direct detection experiments will be sensitive to most of the focus point region of mSUGRA.

In the focus point region, $\sigma_p^{\rm SI}$ is dominated by Higgs-mediated diagrams, and the Higgs-neutralino coupling is sensitively dependent on the sign of μ, producing a suppression of $\sigma_p^{\rm SI}$ in the $\mu < 0$ case relative to the $\mu > 0$ case. For moderate $\tan\beta$ this leads to a relative factor of a few in $\sigma_p^{\rm SI}$, from the coupling coefficients and at large $\tan\beta$ due to the relative contribution of the heavy Higgs-mediated diagrams. Although the general lore holds that $\mu > 0$ is preferable to address the discrepancy in the anomalous magnetic moment of the muon [38–40], in focus point theories the contribution for either sign of μ is too small to produce consistency or to further aggravate the discrepancy without considering significant nonuniversality of smuon masses [41].

Determinations of $\sigma_p^{\rm SI}$ for neutralinos also suffer from the well-known uncertainty in the quark scalar form factor of the nucleons, f_q^N, defined as

$$\langle N | m_q \bar{\psi}_q \psi_q | N \rangle = f_q^N M_N. \tag{10}$$

The form factors for the up- and down-type quarks are well measured, and the heavy quark form factors are determined by loop contributions from the gluon form factor, but there is a longstanding controversy regarding the strange quark form factor, which feeds into $\sigma_p^{\rm SI}$ in a quantitatively important way [42–44]. Older results from chiral perturbation theory [45–47] combined with determination of the nucleon sigma term from meson scattering data [48], and supported by direct computation [49], suggested $f_s = f_s^n = f_s^p \approx 0.36$. For this value of f_s, the other form factors are all much smaller, $f_{q\neq s}^N \lesssim 0.05$, and so the strange quark contribution dominates the direct detection cross section [42]. However, recent lattice studies favor a much smaller value of [50,51]

$$f_s \approx 0.05, \tag{11}$$

much closer to the other quark flavors [43,52]. It has also been argued that the lower value for f_s is consistent with chiral perturbation theory computations, provided higher-order baryon decuplet contributions are taken into account [49,50,53,54]. A recent calculation considering these contributions found $f_s = 0.017 \pm 0.15$ [55]; for similar recent conclusions, see Refs. [56,57]. Here we take $f_s = 0.05$ in deriving direct detection cross sections.

Figure 4 shows exclusion contours for XENON100 in the $(\tan\beta, M_{1/2})$ plane for both signs of μ and $\rho_{\rm local} = 0.3\ {\rm GeV/cm^3}$. For $\mu > 0$, current XENON100 bounds require $M_{1/2} \gtrsim 1.8$ TeV for a wide range of $\tan\beta$, with stronger exclusions at large and small $\tan\beta$, as discussed above. A small region at very large $\tan\beta$ is allowed for $M_{1/2} \gtrsim 500$ GeV; here the lightest neutralino is nearly pure Bino due to the A funnel crossing through the focus point region. For $\mu < 0$, XENON100 requires $M_{1/2} \gtrsim 1.3$ TeV for moderate values of $\tan\beta$, but the exclusions are much weaker for small and large $\tan\beta$. For small $\tan\beta$, this is because of suppression of the dark matter-Higgs coupling from the interplay of the two Higgsino components, and at large $\tan\beta$, it is caused by a cancellation between the light and heavy Higgs diagrams [41]. As a result, large portions of the parameter space remain viable. Exclusion contours for $\rho_{\rm local} = 0.15\ {\rm GeV/cm^3}$ are also presented, motivated by the possibility of a local

[2]The size of the 3-loop corrections is consistent within the uncertainty with the next-to-leading logarithm analysis of Ref. [35], which used a somewhat different organization of the perturbation series.

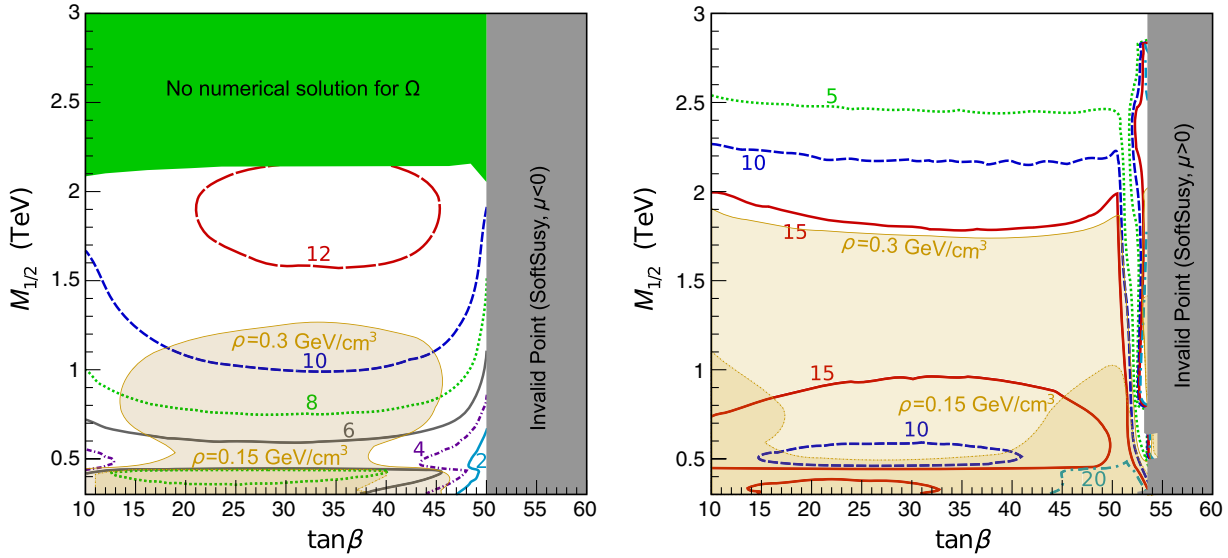

(a) $\mu < 0$ (b) $\mu > 0$

FIG. 4 (color online). Contours of spin-independent scattering cross section σ_p^{SI} in zb. The shaded regions are excluded by XENON100 [37], assuming local dark matter density $\rho_{\mathrm{local}} = 0.3$ GeV/cm^3 (light shaded) and $\rho_{\mathrm{local}} = 0.15$ GeV/cm^3 (dark shaded).

dark matter density somewhat lower than normal due to the presence of the small-scale structure [58]. For this lower value of ρ_{local} and both signs of μ, the excluded region is roughly comparable to that excluded by gluino searches, only becoming stronger for large and small $\tan\beta$ when $\mu > 0$, and almost none of the parameter space preferred by the Higgs mass is excluded by direct detection.

Dark matter may also be detected directly through its spin-dependent couplings. Figure 5 shows contours of constant σ_p^{SD}, the spin-dependent neutralino-proton scattering cross section. Across the parameter space of the focus point region compatible with the correct thermal neutralino relic density, σ_p^{SD} is in the range $10^{-6} - 3 \times 10^{-4}$ pb, for both signs of μ, decreasing with increasing $M_{1/2}$. At large values of $M_{1/2}$, the lightest neutralino becomes increasingly Higgsino-like, suppressing σ_p^{SD}. However, the observed Higgs mass disfavors the pure Higgsino limit, and the 2σ allowed region for m_h favors σ_p^{SD} in the range 10^{-4}–10^{-5} pb.

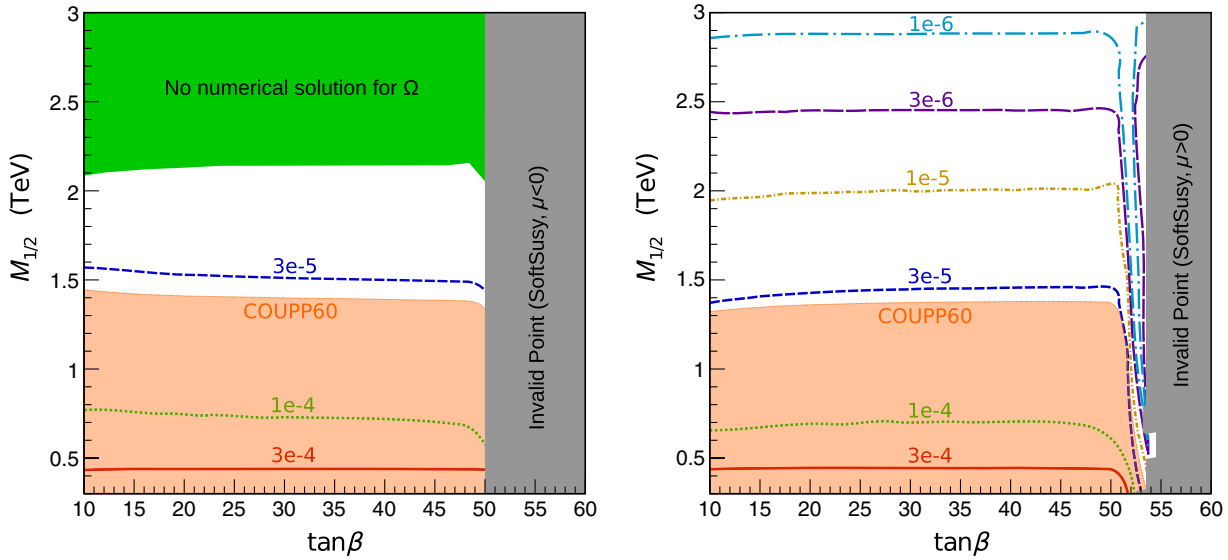

(a) $\mu < 0$ (b) $\mu > 0$

FIG. 5 (color online). Contours of the spin-dependent neutralino-proton scattering cross section σ_p^{SD} in pb. The shaded region indicates the reach of COUPP-60 [59] after 12 months with $\rho_{\mathrm{local}} = 0.3$ GeV/cm^3.

The shaded region shows the sensitivity expected from COUPP-60 [59,60], corresponding to a data-taking period of 12 months at SNOLAB, in the zero-background assumption and using the typical local dark matter density of $\rho_{\rm local} = 0.3\ {\rm GeV/cm^3}$. With one year of data, the COUPP-500 kg experimental sensitivity is anticipated to range between a few $\times\ 10^{-6}$ pb at 100 GeV to a few $\times\ 10^{-5}$ pb at 1 TeV, thus covering a significant portion of the parameter space of interest here.

V. NEUTRINOS FROM ANNIHILATION IN THE SUN AND IN THE EARTH

The search for high-energy neutrinos from the direction of the center of the Sun or of the Earth has a special place in the ranks of indirect detection techniques. In the limit where the capture rate of dark matter particles in celestial bodies is equilibrated by the annihilation rate, the flux of neutrinos solely depends on the scattering cross section of dark matter off of nuclei in the celestial bodies. In the case of the Sun, the dominant scattering mechanism for neutralinos in the minimal supersymmetric standard model is typically spin-dependent scattering, while scattering in the Earth is dominated by spin-independent processes. Unlike searches for antimatter or gamma rays, where the target dark matter densities are generally poorly known and affected by large uncertainties, the flux of neutrinos from the Sun or the Earth has a rather mild dependence on astrophysical inputs. The only crucial information is, in fact, the local dark matter density. In this respect, of all indirect searches, neutrino telescopes provide perhaps the most robust limits.

In Fig. 6 we show the flux of muons produced via charge-current interactions by high-energy neutrinos from dark matter annihilation in the Sun. To calculate this rate (as well as all of the subsequent indirect detection rates) we employ the DARKSUSY package, version 5.0.5 [61]. Figure 6 shows the integrated muon rate for muons with energies larger than 1 GeV. The shaded region at the bottom is excluded by the latest results from 317 days of data taken from 2010–2011 at the IceCube neutrino telescope with the 79-string configuration, and with the use of the DeepCore subarray [62]. This region excludes a parameter space portion comparable to that excluded by current LHC searches. Note that the 1 GeV threshold is much lower than the detector's actual energy threshold, even with the use of DeepCore, but the 1 GeV threshold is used in Ref. [62] for consistency with other results in the field, especially from experiments such as SuperKamiokande, where the 1 GeV threshold is actually experimentally meaningful. For IceCube/DeepCore, the extrapolation below the 1 GeV threshold is made based on the assumed neutrino spectrum, which in the focus point region corresponds closely to the W^+W^- channel for which the exclusion limits are quoted in Ref. [62].

The results of Ref. [62] fell short by about a factor 2–5 of the anticipated target sensitivity quoted in Ref. [63] for 180 days. We find that had the detector performed to the level anticipated in Ref. [63], the exclusion limit would have extended up to $M_{1/2} \approx 1.5$ TeV, covering much of the parameter space of the focus point region compatible with the Higgs mass. This is supported by Fig. 7, where we show the flux of muons integrated above a 100 GeV threshold; these numbers are therefore more indicative of the actual number of events IceCube might detect than those shown by the contours of Fig. 6. The shaded region corresponds to the original 180 days sensitivity target, which would have excluded $M_{1/2} \lesssim 1.5$ TeV with little

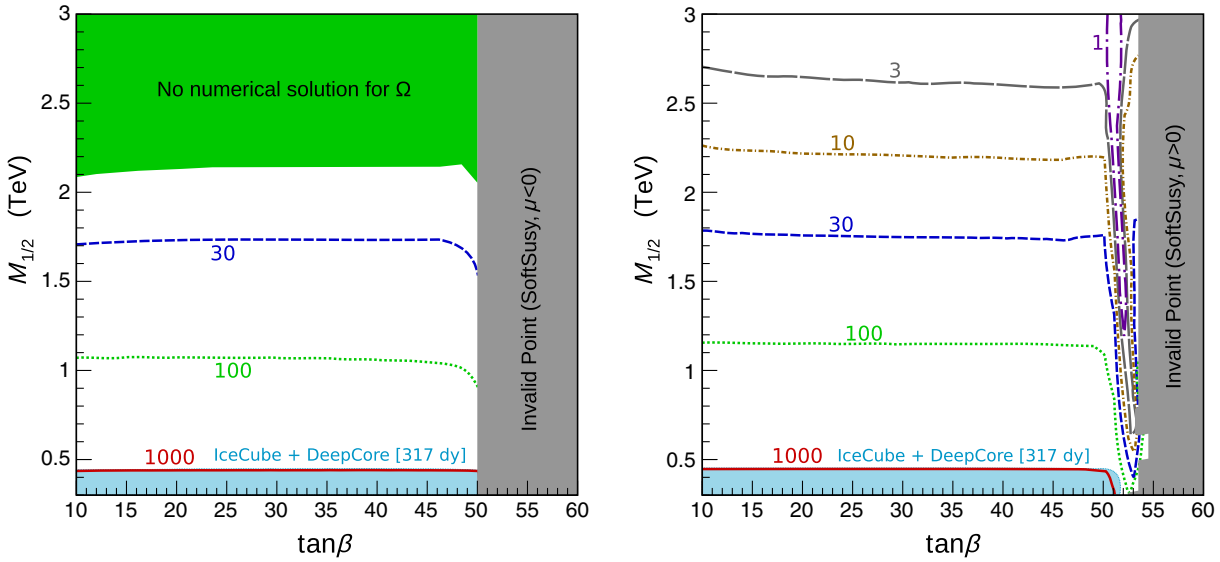

(a) $\mu < 0$ (b) $\mu > 0$

FIG. 6 (color online). The flux of muons in units of $\rm km^{-2}\ yr^{-1}$ with energies above 1 GeV at IceCube. The shaded region is excluded by current limits from IceCube/DeepCore [62].

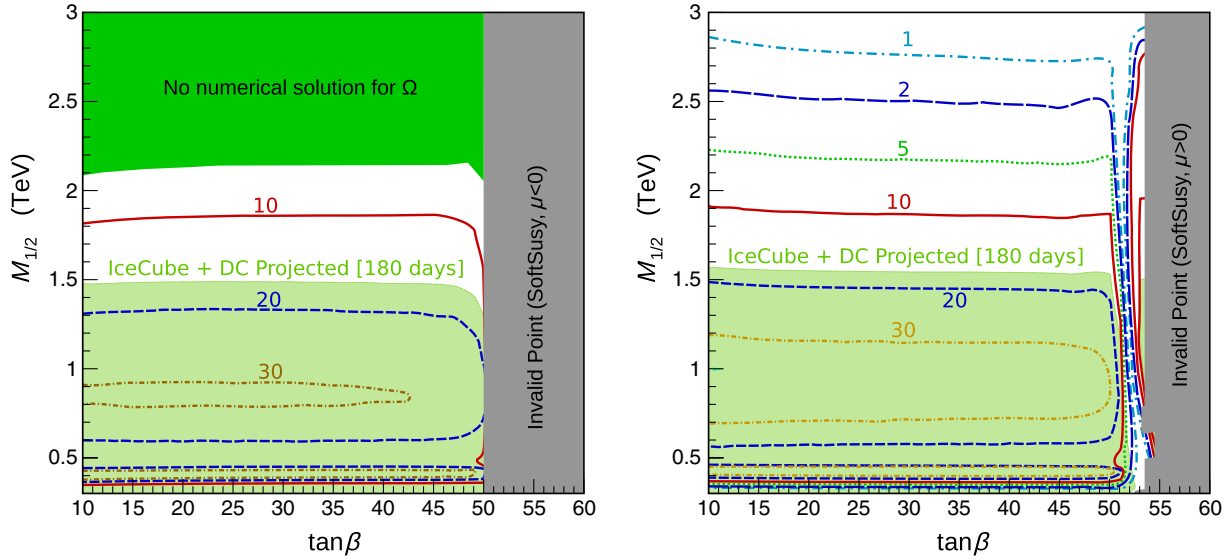

(a) $\mu < 0$ (b) $\mu > 0$

FIG. 7 (color online). The flux of muons in units of $\mathrm{km}^{-2}\,\mathrm{yr}^{-1}$ with energies above 100 GeV at IceCube. The shaded region shows the originally anticipated sensitivity region for 180 live days for the IceCube/DeepCore system [63].

dependence on $\tan\beta$, corresponding to a lightest neutralino mass of ~600 GeV. This emphasizes how promising neutrino telescope searches are in the context of searches for a signal of new physics from the focus point region. We also note that the recent null results from the ANTARES collaboration [64] reinforce the lack of a high-energy neutrino signal from the Sun, at a level very close to the current IceCube/DeepCore limits.

The rates of high-energy neutrinos, and consequently of muons, from neutralino annihilation in the center of the Earth are not nearly as exciting as those from the center of the Sun. We show in Fig. 8 the calculated fluxes of muons from the Earth, again integrated above a 1 GeV energy threshold. Nowhere do we obtain fluxes much larger than 10^{-3} $\mathrm{km}^{-2}\,\mathrm{yr}^{-1}$, which is clearly well below the sensitivity of km^3-sized neutrino telescopes. We note that unlike the case of the Sun, for the Earth the dependence of the flux of neutrinos on the spin-independent cross section induces a significant dependence on the sign of μ, with positive μ producing larger fluxes due to the lack of interfering terms in the neutralino-proton scalar cross section, as discussed in the previous section.

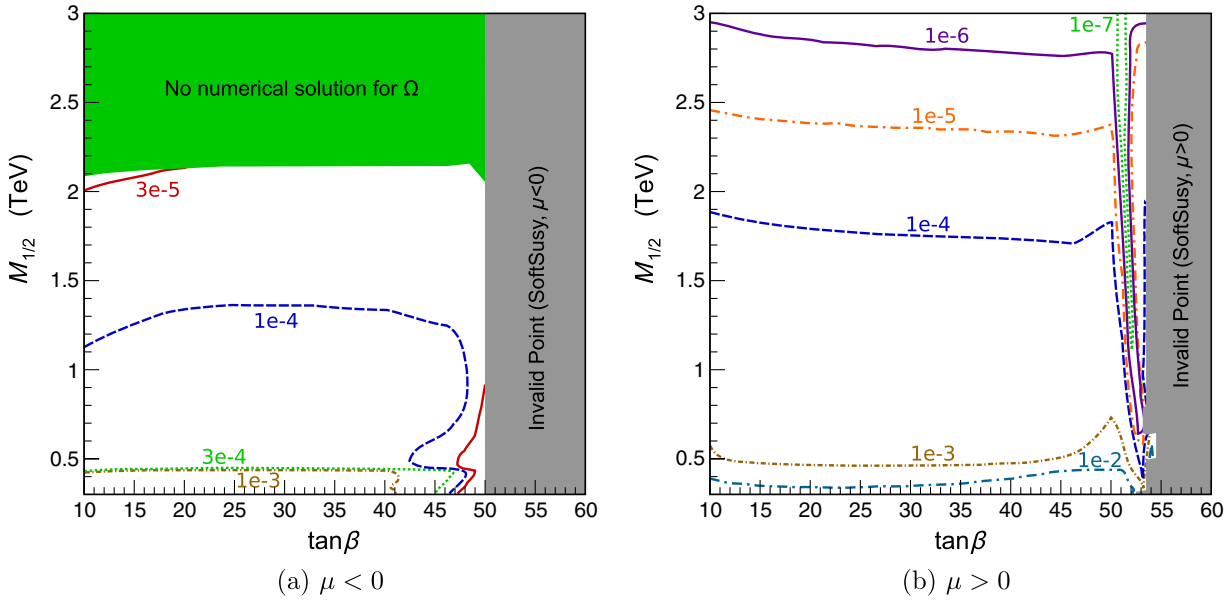

(a) $\mu < 0$ (b) $\mu > 0$

FIG. 8 (color online). The flux of muons in units of $\mathrm{km}^{-2}\,\mathrm{yr}^{-1}$ with energies above 1 GeV at IceCube from dark matter annihilation in the center of the Earth.

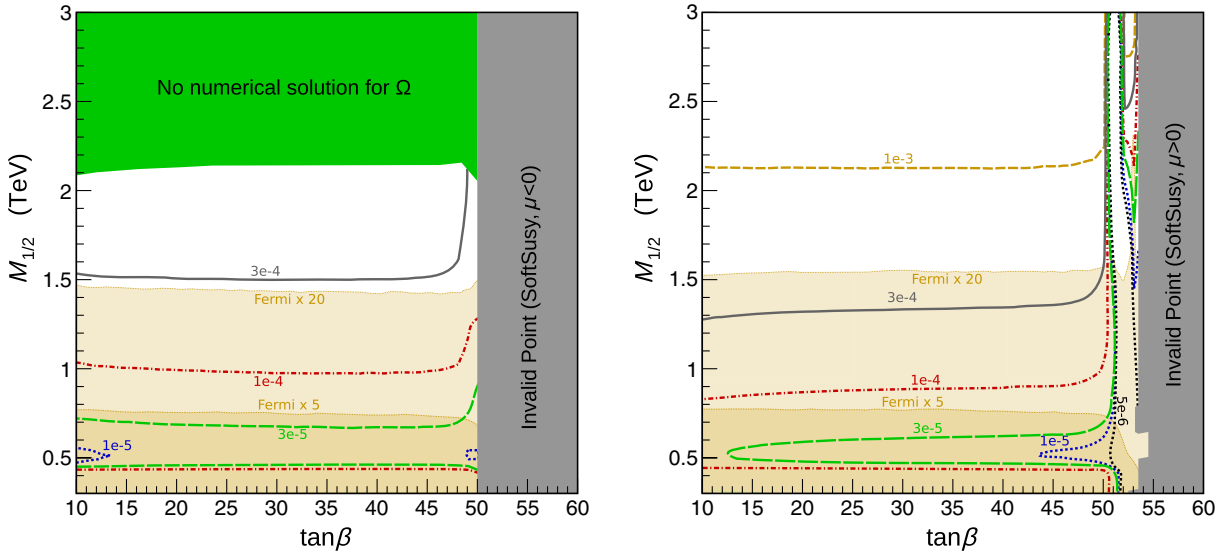

(a) $\mu < 0$ (b) $\mu > 0$

FIG. 9 (color online). Gamma ray searches in the focus point region. The curves indicate constant values for the branching ratio for neutralino pair annihilation into two photons. Null results from Fermi searches for a monochromatic gamma-ray line do not put any constraint on this plane. Null results for continuum gamma-ray signals with Fermi using stacked dwarf galaxies also do not exclude any of this parameter space. However, improvements of current bounds on the gamma-ray continuum will probe the parameter space. The shaded regions indicate the performance of searches for a continuum gamma-ray signal, assuming current sensitivities are improved by factors of 5 and 20, as indicated.

VI. GAMMA RAYS

Gamma rays provide another promising possibility for the indirect detection of dark matter. This signal is especially relevant now that the Fermi Large Area Telescope (LAT) [65] has revolutionized our understanding of the high-energy sky, in a photon energy range extraordinarily relevant for indirect searches for WIMP dark matter.

The gamma-ray signal may take one of two forms. It may appear as a monochromatic line, if photons are produced as one or both of the annihilation products in a two-body final state. Alternatively, the signal may be an excess of continuum gamma rays extending for several decades in energy below the dark matter particle mass. Such continuum gamma rays are typically produced from the two-photon decay of neutral pions resulting from the hadronization of annihilation products, or from final state radiation, or from inverse Compton processes associated with final state electrons and positrons.

We begin by considering the line signal. Figure 9 shows curves of constant branching ratio into two photons. The branching fraction increases towards increasing masses,[3] but is always much smaller than the percent level. In the focus point parameter space, the thermally averaged neutralino pair annihilation cross section always lies at about 1–2 $\times 10^{-26}$ cm^3 s^{-1}, with the mismatch with the canonical value of 3×10^{-26} cm^3 s^{-1} being due to chargino and next-to-lightest neutralino coannihilation. These values imply that the Fermi LAT collaboration line search limits [67] do not yet constrain this parameter space.

The recent discovery of a 130 GeV linelike feature in the Fermi LAT data has attracted great attention [68,69]. Our results indicate that focus point supersymmetry does not provide a viable framework to explain the line feature with dark matter annihilation, as the branching ratio into two photons, and the associated pair-annihilation cross section, are much smaller than the required value of $\sim 10^{-27}$ cm^3 s^{-1}.

Turning next to the continuum signals, we consider annihilation in local dwarf galaxies, currently one of the most stringent and robust limits on the pair-annihilation cross section of dark matter. Cross sections of the order of what the theory predicts over the parameter space of interest are only constrained for neutralino masses on the order of 30 GeV [70]. In focus point supersymmetry, such masses are never consistent with the relic density constraint (and are also excluded by neutrino telescope searches and by LHC results), and the limits weaken approximately quadratically with mass.

This is illustrated with the shaded regions shown in Fig. 9, which indicate the improvement to the Fermi limits needed to probe the parameter space of interest; we indicate the sensitivity lines corresponding to improvements by factors of 5 and 20. In the focus point region, neutralinos

[3]This might be partly due to the fact that the annihilation mode into two photons is the only electroweak one-loop correction implemented in DARKSUSY: this artificially boosts the branching ratio into two photons as the neutralino mass approaches M_W/α_W [66]; this result should therefore be taken with a grain of salt.

pair annihilate with a branching ratio close to 100% into SU(2) gauge boson pairs, WW and ZZ. The two channels produce very similar gamma-ray spectra. To determine the limits from the Fermi combined dwarf observations, we therefore employed the WW final state limits shown in that work. To approach the level of $M_{1/2} \sim 1.5$ TeV, the Fermi limit from stacked dwarf galaxies [70] would need to be improved by a factor of 20. Such an improvement would take a time frame which is beyond the anticipated lifetime of the mission. We note, however, that an improvement of a factor 5 corresponds approximately to observations of the same 10 dSph employed in the current Fermi LAT limits, but for an observation time of 10 years [71].

As presented in Fig. 9, the constraints from gamma-ray observations are notably less effective than those from neutrino telescopes. A comparison between the two methods is not trivial: in all models under consideration here there exists equilibration between neutralino capture and annihilation in the Sun. The neutrino flux from the Sun thus depends almost exclusively on the capture rate which, in turn, depends on the spin dependent scattering cross section. This is an entirely different quantity from the ratio of annihilation rate over neutralino mass squared that enters the Fermi constraints. The large energy threshold for neutrino telescopes also affects the limits in the low-mass region, while no such threshold effect is present for the Fermi limits.

It is important to note, however, that we have considered here line and continuum signals given conservative assumptions. Constraints can be obtained by employing optimistic choices for the density profile of the inner Galaxy, or of external galaxies or clusters, or by utilizing optimistic assumptions for the dark matter substructure content and structure. Here, we have limited ourselves to the more conservative limits obtained by the Fermi collaboration for line signals [67] and continuum signals from stacked dwarfs [70]. We emphasize that had we used the Galactic center and a favorable dark matter density profile, we could have easily reached radically more optimistic conclusions.

We do not show here predictions for the performance of a future Cherenkov Telescope Array (CTA); see, e.g., Ref. [72]. Certain sensitivity estimates for the reach of CTA optimistically carve into the parameter space of the focus point region, for example from observations of the inner Galaxy [72]. Interestingly, CTA will be especially sensitive to WIMP masses in the TeV region, and is thus, in principle, an ideal instrument to look for a signal in the focus point region. Under conservative assumptions, however, CTA, like Fermi, is not guaranteed to detect a signal from dark matter models in the focus point region. In addition, annihilation of a 1 TeV neutralino in the focus point region to the level needed for a detection with CTA would lead to significant low-energy inverse Compton gamma-ray production, which might conflict with existing Fermi LAT limits. We postpone detailed discussion to future work, but we emphasize that CTA will be a key observational tool in the search for particle dark matter in this region, especially if a signal for TeV-mass dark matter were detected in direct detection or neutrino telescope experiments.

VII. ANTIMATTER

The successful deployment of the Alpha Magnetic Spectrometer (AMS-02) on board the International Space Station has boosted hopes and expectations of using cosmic-ray antimatter as a probe of annihilation of Galactic dark matter. In the context of the focus point region, for models with the correct thermal neutralino relic density, the flux of positrons is always too small to be detectable with any significance by current experiments, so we focus here on antiprotons and antideuterons. The latter choice is motivated by the extremely suppressed background rate and great discrimination capabilities against antiprotons that the future General Antiparticle Spectrometer (GAPS) mission promises for antideuterons in the low energy (approximately at or below 1 GeV) range [73,74].

Figure 10 shows the flux of antiprotons at an energy of 19.6 GeV. We use the default propagation parameters for charged cosmic rays in DARKSUSY, as well as the default DARKSUSY [61] dark matter halo density profile. We choose the particular energy of 19.6 GeV for two reasons:

(1) It was shown in Ref. [75] (see Fig. 10, left and Fig. 11, left) that the best signal to background ratio for antiproton searches in the focus point region ranges between 10 and 100 GeV in kinetic energy, with an optimal value of about 20 GeV when factoring in the need to observe a large enough number of signal events.
(2) 19.6 GeV corresponds to the central value of the relevant energy bin reported by the PAMELA collaboration [76]. At that energy, PAMELA quotes a flux of 7.2×10^{-8} GeV^{-1} cm^{-2} s^{-1} sr^{-1}.

The contours in Fig. 10 indicate that the signal-to-noise ratio expected in the "sweet spot" for the antiproton kinetic energy ranges between 2% for very light neutralinos to less than 0.1% for more massive neutralinos. We find almost no variation between negative and positive values of μ. Given the absence of any striking spectral feature in the predicted spectrum of antiprotons in the focus point region [75], and the fact that variations in the cosmic ray antiproton diffusion and energy loss parameters can induce deformation to the background spectrum much larger than the percent level, we conclude that the predicted flux of antiprotons is generically too small to provide a conclusive dark matter detection avenue for neutralinos in the focus point region.

Figure 11 shows the antideuteron flux at 1 GeV. Although the GAPS experiment will primarily target lower energies (likely between 0.1 and 0.3 GeV), the AMS-02

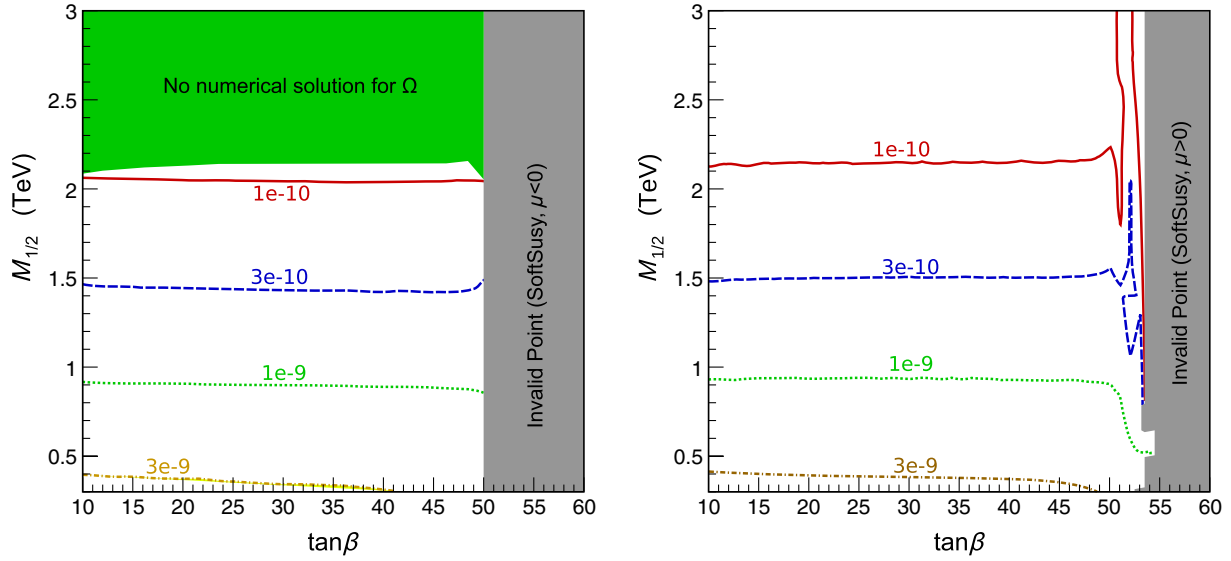

(a) $\mu < 0$ (b) $\mu > 0$

FIG. 10 (color online). The differential flux of antiprotons in units of $\mathrm{GeV}^{-1}\,\mathrm{cm}^{-2}\,\mathrm{s}^{-1}\,\mathrm{sr}^{-1}$ at an energy of 19.6 GeV.

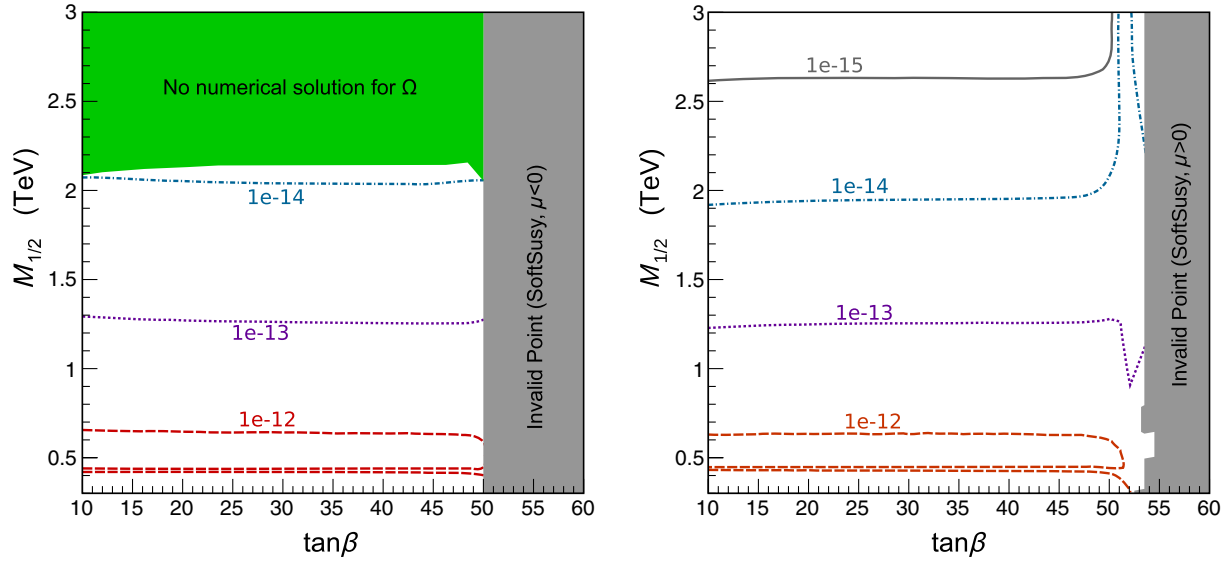

(a) $\mu < 0$ (b) $\mu > 0$

FIG. 11 (color online). The flux of antideuterons at an energy of 1 GeV, in units of $\mathrm{GeV}^{-1}\,\mathrm{cm}^{-2}\,\mathrm{s}^{-1}\,\mathrm{sr}^{-1}$.

limits are likely to be best in the 1 GeV range. In addition, the predicted flux at 0.1–0.3 GeV is typically comparable (within less than a factor 2) to that at 1 GeV for neutralinos in the focus point region.

The GAPS experimental sensitivity target is at present estimated to be at the level of just under $10^{-11}\,\mathrm{GeV}^{-1}\mathrm{cm}^{-2}\mathrm{s}^{-1}\mathrm{sr}^{-1}$, while AMS-02 should be able to reach a sensitivity of about $10^{-10}\ \mathrm{GeV}^{-1}\,\mathrm{cm}^{-2}\,\mathrm{s}^{-1}\,\mathrm{sr}^{-1}$, or approximately an order of magnitude less constraining than GAPS. Figure 11 therefore illustrates that across the relevant focus point region parameter space the expected antideuteron signal is between 1 and 4 orders of magnitude smaller than the best foreseeable experimental sensitivity, making this indirect detection channel inconclusive to search for a dark matter signal.

VIII. DISCUSSION AND CONCLUSIONS

In the context of supersymmetric extensions of the standard model, the discovery of a relatively heavy Higgs boson at the LHC, coupled with null results from superpartner searches, provides strong motivation for considering models with multi-TeV squarks and sleptons. We consider cosmologically motivated focus point model

realizations of this scenario in which dark matter is entirely composed of thermal relics that are mixed Bino-Higgsino or Higgsino-like neutralinos.

Our main findings are the following:

(i) These models remain viable. Claims to the contrary are apparently the result of (a) requiring supersymmetry to resolve the $(g-2)_\mu$ discrepancy (a requirement that is tantamount to considering the standard model to be excluded by this discrepancy), (b) considering only $\mu > 0$ [presumably for historical reasons linked to (a)], (c) using large values of f_s that are now highly disfavored, (d) imposing some highly subjective naturalness criterion, or (e) a combination of these.

(ii) The leading 3-loop $\mathcal{O}(\alpha_t \alpha_s^2)$ contributions to the Higgs mass are positive, lowering the preferred values of scalar masses (possibly to values within reach of the LHC) and improving the fine-tuning of these scenarios.

(iii) Some focus point parameter space is excluded by bounds from direct searches for dark matter, but some remains, including much of the parameter space with $\mu < 0$. In the allowed regions, the predicted spin-independent cross sections are just beyond current bounds from XENON, and spin-dependent scattering is also close to the experimental sensitivity expected in the near future.

(iv) For indirect detection, searches for neutrinos from the core of the Sun at IceCube/DeepCore exclude focus point neutralinos lighter than about 170 GeV. The anticipated detector performance would have placed constraints on neutralinos as heavy as 600 GeV, covering most of the focus point parameter space. There are therefore bright prospects for dark matter discovery through neutrinos at IceCube/DeepCore. Similar sensitivity is being reached by other experiments, such as ANTARES. These results are insensitive to halo model choices, and also do not depend on, e.g., the strange quark content of the proton, and so yield promising probes that are highly complementary to direct detection.

(v) The predicted neutrino flux from the center of the Earth is many orders of magnitude below detectability.

(vi) We have also considered gamma rays from the Galactic center and dwarf galaxies producing either line or continuum signals. Signals in gamma rays are not as promising as in neutrinos, at least for the conservative choices of the relevant dark matter density profiles we employed here, but may nevertheless still be seen in future experiments such as CTA.

(vii) For indirect detection of antiprotons, the signal-to-background ratio, even at optimal energies, is at the percent level and too small to provide a convincing avenue for dark matter detection.

(viii) Antideuteron rates are 1 to 4 orders of magnitude below the foreseen experimental sensitivity of future dedicated experiments, such as GAPS.

To summarize, LHC results so far motivate focus point supersymmetry, which has exciting implications for dark matter searches. Among the most promising are direct searches for spin-independent scattering and indirect searches with neutrino telescopes, but other approaches discussed here may also yield signals. Uncertainties in the Higgs mass calculation also leave open the possibility that squarks and gluinos may be within reach of the LHC, even without large left-right stop mixing. If focus point supersymmetry is realized in nature and focus point neutralinos make up all of the dark matter in the Universe, a signal in one or more of the complementary probes (colliders, direct detection, and indirect detection) will appear in the coming few years.

ACKNOWLEDGMENTS

P. D. and S. P. are partly supported by the U.S. Department of Energy under Contract No. DE-FG02-04ER41268. J. L. F. is supported in part by NSF Grant No. PHY-0970173 and a Simons Foundation Fellowship. D. S. is supported in part by the U.S. Department of Energy under Contract No. DE-FG02-92ER40701 and by the Gordon and Betty Moore Foundation through Grant No. 776 to the Caltech Moore Center for Theoretical Cosmology and Physics. P. K. is supported by the DFG through SFB/TR-9 and by the Helmholtz Alliance "Physics at the Terascale."

[1] J. L. Feng, K. T. Matchev, and T. Moroi, Phys. Rev. Lett. **84**, 2322 (2000).

[2] J. L. Feng, K. T. Matchev, and T. Moroi, Phys. Rev. D **61**, 075005 (2000).

[3] G. Aad *et al.* (ATLAS Collaboration), Phys. Lett. B **716**, 1 (2012).

[4] S. Chatrchyan *et al.* (CMS Collaboration), Phys. Lett. B **716**, 30 (2012).

[5] L. Randall and R. Sundrum, Nucl. Phys. **B557**, 79 (1999).

[6] G. F. Giudice, M. A. Luty, H. Murayama, and R. Rattazzi, J. High Energy Phys. 12 (1998) 027.

[7] J. L. Feng, K. T. Matchev, and F. Wilczek, Phys. Lett. B **482**, 388 (2000).

[8] J. L. Feng, K. T. Matchev, and F. Wilczek, Phys. Rev. D **63**, 045024 (2001).

[9] S. Akula, P. Nath, and G. Peim, Phys. Lett. B **717**, 188 (2012).
[10] O. Buchmueller, R. Cavanaugh, M. Citron, A. De Roeck, M. Dolan *et al.*, Eur. Phys. J. C **72**, 2243 (2012).
[11] H. Baer, V. Barger, P. Huang, D. Mickelson, A. Mustafayev, and X. Tata, Phys. Rev. D **87**, 035017 (2013).
[12] C. Strege, G. Bertone, F. Feroz, M. Fornasa, R. Ruiz de Austri, and R. Trotta, J. Cosmol. Astropart. Phys. 04 (2013) 013.
[13] R. Harlander, P. Kant, L. Mihaila, and M. Steinhauser, Phys. Rev. Lett. **100**, 191602 (2008).
[14] P. Kant, R. Harlander, L. Mihaila, and M. Steinhauser, J. High Energy Phys. 08 (2010) 104.
[15] S. Mizuta and M. Yamaguchi, Phys. Lett. B **298**, 120 (1993).
[16] J. L. Feng and D. Sanford, J. Cosmol. Astropart. Phys. 05 (2011) 018.
[17] E. Komatsu *et al.* (WMAP Collaboration), Astrophys. J. Suppl. Ser. **192**, 18 (2011).
[18] P. Ade *et al.* (Planck Collaboration), arXiv:1303.5076.
[19] J. L. Feng and D. Sanford, Phys. Rev. D **86**, 055015 (2012).
[20] E. Dudas, A. Linde, Y. Mambrini, A. Mustafayev, and K. A. Olive, Eur. Phys. J. C **73**, 2268 (2013).
[21] J. L. Evans, M. Ibe, K. A. Olive, and T. T. Yanagida, arXiv:1302.5346.
[22] B. Allanach, Comput. Phys. Commun. **143**, 305 (2002).
[23] G. Belanger, F. Boudjema, P. Brun, A. Pukhov, S. Rosier-Lees, P. Salati, and A. Semenov, Comput. Phys. Commun. **182**, 842 (2011).
[24] G. Aad (ATLAS Collaboration), Technical Report, 2012.
[25] J. L. Feng, arXiv:1302.6587.
[26] J. R. Ellis, K. Enqvist, D. V. Nanopoulos, and F. Zwirner, Mod. Phys. Lett. A **01**, 57 (1986).
[27] R. Barbieri and G. Giudice, Nucl. Phys. **B306**, 63 (1988).
[28] E. Mountricha (ATLAS Collaboration), "Study of Higgs Production in Bosonic Decays Channels in ATLAS," at the Rencontres de Moriond, 2013 [http://moriond.in2p3.fr/QCD/2013/MorQCD13Prog.html].
[29] C. Ochando (CMS Collaboration), "Study of Higgs Production in Bosonic Decays Channels in CMS," at the Rencontres de Moriond, 2013 [http://moriond.in2p3.fr/QCD/2013/MorQCD13Prog.html].
[30] J. L. Feng, P. Kant, S. Profumo, and D. Sanford, arXiv:1306.2318.
[31] M. Frank, T. Hahn, S. Heinemeyer, W. Hollik, H. Rzehak, and G. Weiglein, J. High Energy Phys. 02 (2007) 047.
[32] G. Degrassi, S. Heinemeyer, W. Hollik, P. Slavich, and G. Weiglein, Eur. Phys. J. C **28**, 133 (2003).
[33] S. Heinemeyer, W. Hollik, and G. Weiglein, Eur. Phys. J. C **9**, 343 (1999).
[34] S. Heinemeyer, W. Hollik, and G. Weiglein, Comput. Phys. Commun. **124**, 76 (2000).
[35] S. P. Martin, Phys. Rev. D **75**, 055005 (2007).
[36] E. Aprile *et al.* (XENON100 Collaboration), Phys. Rev. Lett. **107**, 131302 (2011).
[37] E. Aprile *et al.* (XENON100 Collaboration), Phys. Rev. Lett. **109**, 181301 (2012).
[38] G. Bennett *et al.* (Muon $g-2$ Collaboration), Phys. Rev. D **73**, 072003 (2006).
[39] M. Davier, A. Hoecker, B. Malaescu, and Z. Zhang, Eur. Phys. J. C **71**, 1515 (2011).
[40] F. Jegerlehner and R. Szafron, Eur. Phys. J. C **71**, 1632 (2011).
[41] J. L. Feng, K. T. Matchev, and D. Sanford, Phys. Rev. D **85**, 075007 (2012).
[42] J. R. Ellis, K. A. Olive, and C. Savage, Phys. Rev. D **77**, 065026 (2008).
[43] J. Giedt, A. W. Thomas, and R. D. Young, Phys. Rev. Lett. **103**, 201802 (2009).
[44] O. Buchmueller, R. Cavanaugh, D. Colling, A. De Roeck, M. Dolan *et al.*, Eur. Phys. J. C **71**, 1722 (2011).
[45] B. Borasoy and U.-G. Meissner, Ann. Phys. (N.Y.) **254**, 192 (1997).
[46] J. Gasser, H. Leutwyler, and M. Sainio, Phys. Lett. B **253**, 260 (1991).
[47] V. Bernard, N. Kaiser, and U.-G. Meissner, Phys. Lett. B **389**, 144 (1996).
[48] M. Pavan, I. Strakovsky, R. Workman, and R. Arndt, PiN Newslett. **16**, 110 (2002).
[49] J. Alarcon, J. M. Camalich, and J. Oller, Phys. Rev. D **85**, 051503 (2012).
[50] R. Young and A. Thomas, Phys. Rev. D **81**, 014503 (2010).
[51] W. Freeman and D. Toussaint, Proc. Sci., LAT2009 (2009) 137 [arXiv:0912.1144].
[52] A. Thomas, P. Shanahan, and R. Young, Few-Body Syst. **54**, 123 (2013).
[53] E. E. Jenkins and A. V. Manohar, Phys. Lett. B **281**, 336 (1992).
[54] V. Bernard, N. Kaiser, and U. G. Meissner, Z. Phys. C **60**, 111 (1993).
[55] J. Alarcon, L. Geng, J. M. Camalich, and J. Oller, Phys. Rev. D **87**, 114510 (2013).
[56] P. Junnarkar and A. Walker-Loud, arXiv:1301.1114.
[57] R. Young, Proc. Sci., LATTICE2012 (2012) 014 [arXiv:1301.1765].
[58] M. Kamionkowski and S. M. Koushiappas, Phys. Rev. D **77**, 103509 (2008).
[59] E. Ramberg (COUPP Collaboration), Nucl. Instrum. Methods Phys. Res., Sect. A **623**, 454 (2010).
[60] E. Vazquez Jauregui (COUPP Collaboration), "COUPP500: A 500 kg Bubble Chamber for Dark Matter Detection," at the IDM2012, 2012 [http://kicp-workshops.uchicago.edu/IDM2012/depot/talk-vazquez-jauregui-eric__1.pdf].
[61] P. Gondolo, J. Edsjo, P. Ullio, L. Bergstrom, M. Schelke, and E. A. Baltz, J. Cosmol. Astropart. Phys. 07 (2004) 008.
[62] M. Aartsen *et al.* (IceCube Collaboration), Phys. Rev. Lett. **110**, 131302 (2013).
[63] R. Abbasi *et al.* (IceCube Collaboration), Phys. Rev. D **85**, 042002 (2012).
[64] S. Adrian-Martinez *et al.* (ANTARES Collaboration), arXiv:1302.6516.
[65] W. Atwood *et al.* (LAT Collaboration), Astrophys. J. **697**, 1071 (2009).
[66] J. Hisano, S. Matsumoto, and M. M. Nojiri, Phys. Rev. D **67**, 075014 (2003).

[67] M. Ackermann *et al.* (LAT Collaboration), Phys. Rev. D **86**, 022002 (2012).
[68] T. Bringmann, X. Huang, A. Ibarra, S. Vogl, and C. Weniger, J. Cosmol. Astropart. Phys. 07 (2012) 054.
[69] C. Weniger, J. Cosmol. Astropart. Phys. 08 (2012) 007.
[70] A. Abdo *et al.* (Fermi-LAT Collaboration), Astrophys. J. **712**, 147 (2010).
[71] A. Morselli, E. Nuss, and G. Zaharijas (Fermi-LAT Collaboration), arXiv:1305.7173.
[72] M. Doro *et al.* (CTA Collaboration), Astropart. Phys. **43**, 189 (2013).
[73] C. Hailey, T. Aramaki, S. Boggs, P. Doetinchem, H. Fuke *et al.*, Adv. Space Res. **51**, 290 (2013).
[74] H. Baer and S. Profumo, J. Cosmol. Astropart. Phys. 12 (2005) 008.
[75] H. Baer, T. Krupovnickas, S. Profumo, and P. Ullio, J. High Energy Phys. 10 (2005) 020.
[76] O. Adriani *et al.* (PAMELA Collaboration), Phys. Rev. Lett. **105**, 121101 (2010).